energies

MDPI

Article

The Thermodynamic and Kinetic Effects of Sodium Lignin Sulfonate on Ethylene Hydrate Formation

Yiwei Wang [1], Lin Wang [2], Zhen Hu [2], Youli Li [2], Qiang Sun [2], Aixian Liu [1], Lanying Yang [2], Jing Gong [3] and Xuqiang Guo [1,*]

[1] State Key Laboratory of Heavy Oil Processing, China University of Petroleum Beijing at Karamay, Karamay 834000, China; wyw@cup.edu.cn (Y.W.); 1855@cupk.edu.cn (A.L.)
[2] State Key Laboratory of Heavy Oil Processing, China University of Petroleum (Beijing), Beijing 102249, China; 2018216540@student.cup.edu.cn (L.W.); 2018213529@student.cup.edu.cn (Z.H.); 2018216539@student.cup.edu.cn (Y.L.); sunq@cup.edu.cn (Q.S.); yanglanying@cup.edu.cn (L.Y.)
[3] National Engineering Laboratory for Pipeline Safety/MOE Key Laboratory of Petroleum Engineering/Beijing Key Laboratory of Urban Oil and Gas Distribution Technology, China University of Petroleum (Beijing), Beijing 102249, China; ydgj@cup.edu.cn
* Correspondence: guoxq@cup.edu.cn; Tel.: +86-0990-6633300

Abstract: Hydrate-based technologies (HBTs) have high potential in many fields. The industrial application of HBTs is limited by the low conversion rate of the water into hydrate (R_{WH}), and sodium lignin sulfonate (SLS) has the potential to solve the above problem. In order to make the HBTs in the presence of SLS applied in industry and promote the advances of commercial HBTs, the effect of SLS on the thermodynamic equilibrium hydrate formation pressure (P_{eq}) was investigated for the first time, and a new model (which can predict the P_{eq}) was proposed to quantitatively describe the thermodynamic effect of SLS on the hydrate formation. Then, the effects of pressure and initial SLS concentration on the hydrate formation rate (r_R) at different stages in the process of hydrate formation were investigated for the first time to reveal the kinetic effect of SLS on hydrate formation. The experimental results show that SLS caused little negative thermodynamic effect on hydrate formation. The P_{eq} of the ethylene-SLS solution system predicted by the model proposed in this work matches the experimental data well, with an average relative deviation of 1.6% and a maximum relative deviation of 4.7%. SLS increased R_{WH}: the final R_{WH} increased from 57.6 ± 1.6% to higher than 70.0% by using SLS, and the highest final R_{WH} (77.0 ± 2.1%) was achieved when the initial SLS concentration was 0.1 mass%. The r_R did not significantly change as R_{WH} increased from 35% to 65% in the formation process in the presence of SLS. The effect of increasing pressure on increasing r_R decreased with the increase in R_{WH} when R_{WH} was lower than 30%, and the difference in pressure led to little difference in the r_R when R_{WH} was higher than 30%.

Keywords: hydrate; thermodynamics; kinetics; sodium lignin sulfonate; model

Citation: Wang, Y.; Wang, L.; Hu, Z.; Li, Y.; Sun, Q.; Liu, A.; Yang, L.; Gong, J.; Guo, X. The Thermodynamic and Kinetic Effects of Sodium Lignin Sulfonate on Ethylene Hydrate Formation. *Energies* **2021**, *14*, 3291. https://doi.org/10.3390/en14113291

Academic Editors: Jiafei Zhao, Yue Hu and Jacek Majorowicz

Received: 5 May 2021
Accepted: 1 June 2021
Published: 4 June 2021

1. Introduction

Clathrate hydrates are crystal inclusion compounds which are made up of water molecules and guest molecules (such as CH_4, C_2H_4, CO_2, etc.) [1]. The guest gas molecules are captured into hydrate cages by van der Waal interaction forces [2], and the water molecules in clathrate hydrates are connected by hydrogen bonds [3]. The three common hydrate structures are cubical structure I (sI), cubical structure II (sII) and hexagonal structure H (sH) [4]. Due to the properties of clathrate hydrate shown in the literature (such as environmental friendliness [5], high gas storage capacity [6], different selectivity on gas species [7], moderate operating condition [7], high energy content [8] and non-explosive nature [9]), hydrate-based technologies have been proved to have high potential in many fields, such as carbon dioxide capture [10], gas separation [11], gas storage/transportation [12], water desalination [13] and cold storage [8]. However, few

hydrate-based technologies have been commercially applied [14], because the conversion rate of the water into hydrate (R_{WH}) is not high enough to meet the demands of the commercial applications [9]. For that reason, how to increase R_{WH} through a cheap method is the key concern in the advances in gas hydrate technologies.

One of the most effective and cheap methods to increase R_{WH} is using surfactants [15]. Instead of increasing R_{WH} by participating in hydrate formation such as thermodynamic promoters, surfactants increase R_{WH} by improving the mass transfer between gas phase and liquid phase [16] as well as preventing the agglomeration of hydrate particles [17]. As a surfactant with high degree of dispersion [18], sodium lignin sulfonate (SLS) has received a lot of attention due to its environmentally friendly nature, nontoxic nature, low price and high water solubility [19]. Compared with sodium dodecyl sulfonate (SDS), which is the most-used surfactant in hydrate formation [20], SLS has a lower foaming ability [21]. Since foams not only reduce the performances of hydrate-based gas storage and hydrate-based gas transportation, but also make the dissociated gas in hydrate difficult to release [22], using SLS instead of SDS in hydrate-based technologies can reduce the negative effect of foams on hydrate-based technologies. On the other hand, SLS is a byproduct of paper manufacturing [23]. The global paper industry produces 50 million tons of SLS annually [19]. However, only 5% of SLS is commercially used (as additives, dispersants, binders and surfactants); the rest is burned to recover energy or discharged into water, which causes not only a waste of resource but also an environmental problem [24]. For the above reason, the utilization of SLS in hydrate-based technologies has significance in the fields of resource recovery and environmental protection.

The increase in R_{WH} during the hydrate formation process leads to changes of the liquid composition, the mass transfer resistance, and the fluidity of hydrate slurry, which cause changes of the thermodynamic effect (which manifests as the effect of SLS on thermodynamic equilibrium hydrate formation pressure (P_{eq})) and kinetic effects (which manifests as the effects of SLS on the hydrate formation rate and the final R_{WH} in the hydrate formation controlled by mass transfer) of SLS on hydrate formation. Though SLS has been proven to be effective in enhancing the performances of hydrate-based gas separation [21] and gas storage [25], the thermodynamic effect of SLS on hydrate formation and the thermodynamic model, as well as the effects of thermodynamic hydrate formation driving force (THFDF) and initial SLS concentration ($w_{p,0}$) on the hydrate formation rate (r_R) at different stages (described using the value of R_{WH}) in the process of hydrate formation still has not been reported. In order to promote the commercial application of hydrate-based technologies and the advances of hydrate-based technologies, the thermodynamic effect of SLS on the hydrate formation was investigated for the first time (Section 2.2), a new thermodynamic model was proposed to quantitatively describe the thermodynamic effect of SLS on the hydrate formation (Section 3), the interfacial tension of ethylene gas-SLS solution was investigated for the first time (Section 2.3) and the effects of THFDF and $w_{p,0}$ on the r_R at different stages in the process of the hydrate formation was investigated for the first time (Section 2.4).

Since most of the gases (fluid catalytic cracking dry gas [15], methane gas [26], etc. [27]) in the research papers that focused on hydrate-based gas separation/storage form structure I hydrates in the absence of thermodynamic promoter, and R_{WH} is necessary for the quantitative description of the stages in the process of hydrate formation, ethylene was chosen as the experimental gas in this work, because pure ethylene gas forms structure I hydrate, and the R_{WH} can be accurately calculated using the amount of the ethylene in the hydrate [15]. The ratio of ethylene-to-water molecular numbers in ethylene hydrate is a fixed constant [27], because the ratio of large cavity-to-water molecule numbers in structure I hydrate is a fixed constant [27], ethylene molecules can only occupy the large cavity of hydrate [27] and every large cavity is filled by one ethylene molecule [28]. In the hydrate formed by the gases (CH_4, CO_2, etc.) that can occupy both the small cavities and the large cavities of structure I hydrate [5], the fraction of the small cavities filled by gas molecules (θ) is variable and is affected by many influential factors (temperature, pressure, kinetic

conditions, etc.) [29], so that the gas-to-water ratio of molecular numbers in the hydrate is variable, which is why R_{WH} cannot be accurately calculated. It needs to be pointed out that the relationship between the r_R and the R_{WH} is different from the relationship between the r_R and the amount of the gas in the hydrate formed by the gases that can occupy both the small cavities and the large cavities. Because the θ is variable, the amount of the gas in the hydrate in experiment A can be higher than the amount of gas in the hydrate in experiment B when the R_{WH} in experiment A is lower than the R_{WH} in experiment B.

Surfactants do not form hydrate [15] and the concentration of the SLS in the liquid phase (w_p) increases as R_{WH} increases, so that the thermodynamic effect of SLS on hydrate formation increases as R_{WH} increases. Since SLS is a kind of salt, it might have a considerable negative thermodynamic effect on hydrate formation when R_{WH} is high [30]. In addition, the effect of SLS on the hydrate formation in Section 4.3 is the combination of the thermodynamic and kinetic effects of SLS on hydrate formation, so that the kinetic effects would be easy to investigate when the thermodynamic effect is known. For the above reasons, the thermodynamic effect of SLS on hydrate formation was investigated in Section 4.1 before the investigation in Section 4.3 was carried out. Since the gas–liquid interfacial tension is necessary for the discussion on the kinetic effect of SLS on hydrate formation, the interfacial tension between ethylene gas and SLS solution was investigated in Section 4.2. Since the difference between the final state of the hydrate formation and the state of thermodynamic phase equilibrium needs to be quantitatively described in the discussion in Section 4.3, the thermodynamic phase equilibrium pressure under the condition at the end of the hydrate formation ($P_{eq,end}$) needs to be calculated, so that a prediction model of the ethylene–SLS solution system is necessary.

The two most used mechanism models in hydrate formation are the van der Waals-Platteeuw (vdW-P) model [31] and Chen-Guo model [32], which are the foundation of most hydrate formation models. Both the vdW-P model and Chen-Guo model assume that: (a) one hydrate cavity contains at most one guest molecule, (b) the guest molecule-guest molecule interaction can be neglected and (c) the effects of the encaged guest molecules on the hydrate host lattice can be neglected [31,32]. Those assumptions make model calculations simple but at the same time limits the application range and the prediction accuracy of hydrate formation models. In the hydrates formed by small gas molecules, such as hydrogen, oxygen and nitrogen, one cavity can capture two or more than two gas molecules under specific conditions [33]. For example, in the hydrogen hydrate (structure II) formed at 260 K under 20 MPa, more than 80% of the large cavities are occupied by more than one hydrogen molecules [34]. The literature also shows that the guest molecule–host molecule interaction [35], guest molecule–guest molecule interaction [33] and the host relaxation [33] can significantly affect the structure of the hydrate and properties of the corresponding systems.

Many investigations have been done to overcome the limitations caused by the above assumptions. For the models based on the vdW-P theory, the most effective method to overcome the limitations caused by the above assumptions is introducing the host lattice relaxation, guest–guest interactions, guest–host interactions, the quantum nature of guest behavior and the possibility of occupation of single cage by several guests into the method for calculating the chemical potential of water in hydrate [34,36–38], and the models using that method work very well on predicting the phase equilibrium conditions of methane/xenon -hydrate-ice Ih system [36], argon/krypton -hydrate-ice Ih system [38], hydrogen/(hydrogen+propane)-hydrate-ice Ih system [34], helium-ice based hydrate-ice systems [37] and so on. For the models based on the Chen-Guo theory, the host lattice relaxation, guest–host interactions and the quantum nature of guest behavior are introduced into the models by introducing an Antoine-type equation into the calculation of the fugacity of the components in hydrate, and the Antoine parameters are fitted using the pure gas hydrate formation data for a particular structure only [39]. The guest–guest interaction between the guest molecules in small cavities and in large cavities are introduced into models by introducing a correction term into the calculation of the fugacity

of the components in hydrate, and the parameters in the correction term are fitted using experimental data [39]. The possibility of the occupation of a single cage by several guests into the calculation has not been introduced into the models based on the Chen-Guo theory so far.

The number of the parameters required in the Chen-Guo model is less than that of the parameters required in the vdW-P model, which makes the calculations of new systems in the Chen-Guo model simple [31,39]. Since SLS is a new prompter for the hydrate formation model and the occupation of a single cage by several ethylene molecules does happen in the formation of ethylene hydrate (multiple occupancies by carbon dioxide and methane are not supported by experimental data, and the size of ethylene molecule is larger than those of carbon dioxide and methane) [27,33], the Chen-Guo model was chosen to describe the hydrate formation process in the new model in this work, which is described in Section 3 and validated in Section 4.1. It needs to be pointed out that, in the assumptions of the Chen-Guo model, the first step is always the formation of large cavities, which is not in the assumptions of the vdW-P model [31,39]. Though that assumption makes the calculation process of the Chen-Guo model simple, it may limit the application range of the model.

2. Materials and Methods

2.1. Materials and Apparatus

The SLS (purity 96%) was provided by Sinopharm Chemical Reagent Co., Ltd (Beijing, China). The ethylene gas (purity 99.99%) was provided by Beijing AP Beifen Gas Industry Company (Beijing, China). The deionize water (18×10^6 Ω·cm) and SLS were weighed by an electronic balance (±0.1 mg uncertainty).

The experimental apparatus used in Sections 2.2 and 2.4 is shown in Figure 1. The maximum volume of the variable cell is 665.0 mL. The uncertainty of the measured temperature inside the crystallizer is ±0.05 K. The uncertainty of the measured pressure inside the crystallizer is ±0.005 MPa.

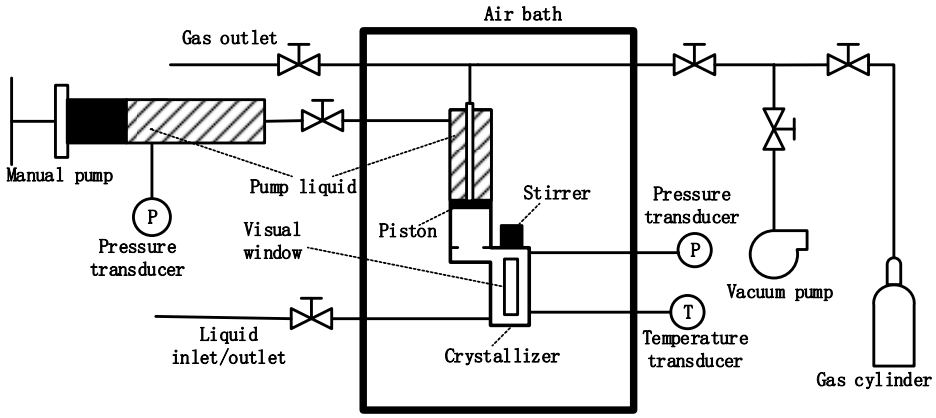

Figure 1. The experimental apparatus for the experiments in Sections 2.2 and 2.4.

When the crystallizer is isolated from the outside, the pressure inside the crystallizer can be increased/decreased by decreasing/increasing the volume of the crystallizer. The volume of the crystallizer is adjusted by adjusting the position of the piston inside the crystallizer, and the position of the piston is adjusted by using the manual pump with scale division lines (±0.05 mL uncertainty).

2.2. The Measurement of P_{eq}

The method for measuring the P_{eq} of the ethylene gas + SLS solution/pure water system in this work is reported in detail in the literature [15], and the reliability of the method has been ensured in the literature published by this laboratory [40,41]. The experiment under each operating condition was repeated three times to ensure the repeatability of the experimental data.

2.3. Interfacial Tension Measurement

The experimental apparatus and procedures in this section are the same as those reported in the literature published by this laboratory [42,43]. In order to ensure the repeatability of the experimental data, the experiment was repeated at least four times under each experimental condition.

2.4. Ethylene Hydrate Formation in the Presence of SLS

The experimental procedure is briefly described as follows:

1. The crystallizer was washed and dried before each experiment.
2. The temperature inside the crystallizer was kept at the experimental temperature.
3. A total of 40 mL SLS solution/pure water was injected from the liquid inlet into the crystallizer.
4. The air inside the crystallizer was completely replaced by ethylene gas.
5. The temperature inside the crystallizer was kept at the experimental temperature.
6. Ethylene gas was injected into the crystallizer to increase the pressure.
7. Once the pressure inside the crystallizer reached the experimental value, the valves of the crystallizer were closed to isolate the crystallizer from the outside. The stirrer was set at a constant speed of 500 rpm. This moment was noted as the start of a hydrate formation experiment.
8. Along with the consumption of the ethylene gas by hydrate formation, the pressure inside the crystallizer was kept constant by decreasing the volume of the crystallizer. The data of time vs. the volume of the crystallizer was recorded.
9. When the volume of the crystallizer remained constant for at least 2 h, the hydrate formation was considered to have ended.
10. The experiment under each operating condition was repeated three times.

2.5. Ethylene Hydrate Formation in the Presence of SLS

The amount of the ethylene in the hydrate slurry at time t ($N_{d,t}$, mol) can be calculated by Equation (1):

$$N_{d,t} = [P_f \cdot (V_{cr,0} - V_{cr,t})] / (Z \cdot R \cdot T_f) \quad (1)$$

where $V_{cr,0}$ is the volume of the crystallizer at the beginning of the hydrate formation, $V_{cr,t}$ is the volume of the crystallizer at the time t in the hydrate formation, P_f and T_f are the experimental pressure and temperature, respectively, and they are kept constant in each individual experiment, R is 8.3145 J·mol^{-1}·K^{-1} and Z is the compressibility factor of the gas inside the crystallizer under the experimental condition, which is calculated by Patel-Teja EOS [44]. The gas storage capacity of the hydrate slurry (*GSCHS*, NL/L) is calculated by Equation (2):

$$GSCHS = (Z_{st} \cdot N_{d,end} \cdot R \cdot T_{st}) / (P_{st} \cdot V_{sol}) \quad (2)$$

where V_{sol} is the volume of the SLS solution/pure water at the beginning of an experiment, P_{st} is 101,325 Pa, T_{st} is 273.15 K, $N_{d,end}$ is the amount of the ethylene in the hydrate slurry at the end of the hydrate formation and Z_{st} is the compressibility factor of the ethylene gas under 273.15 K, 101325 Pa. The hydrate formation rate ($r_{R=X}$,%/min) when R_{WH} is X (%) is calculated as the average formation rate during the period that R_{WH} increases from X − 1.0% to X + 1.0%:

$$r_{R=X} = \frac{(X + 1.0\%) - (X - 1.0\%)}{t_{(X+1.0\%)} - t_{(X-1.0\%)}} \quad (3)$$

where $t_{(X+1.0\%)}$ is the time when R_{WH} is X + 1.0% and $t_{(X-1.0\%)}$ is the time when R_{WH} is X − 1.0%. The average data ($\overline{Data}$) and the uncertainty for the repeated experiments ($Data_u$) are calculated as follows:

$$\overline{Data} = \sum Data_{jjj} / jj \quad (4)$$

$$Data_u = \max\left\{\left|Data_{max} - \overline{Data}\right|, \left|\overline{Data} - Data_{min}\right|\right\} \quad (5)$$

The experiment, under each operating condition, was repeated *jj* times to ensure repeatability. *jj* is 4 for the experiments in Sections 3 and 4.2 for the experiments in Sections 4.1 and 4.3. *jjj* is the sequence number. $Data_{max}$ and $Data_{min}$ are the maximum value and minimum value of a data in *jj* times repeated experiments, respectively.

3. Modeling

The model in this work uses "the difference in chemical potentials is zero when pressure is P_{eq}" [15] as the convergence condition of the iterative algorithm and uses Modified PT EOS [45] to introduce the thermodynamic effect of SLS on the hydrate formation into the model, which distinguishes the model in this work from the other models based on the Chen-Guo two-step hydrate formation mechanism [32,39].

The first step in the Chen-Guo two-step hydrate formation mechanism is the formation of basic hydrate (the small cavities are all empty): each ethylene molecule in liquid phase forms an unstable molecular cluster with the water molecules nearby, and this molecular cluster is the structure of the large cavity. As discussed in the Introduction, one large cavity is occupied by one ethylene molecule. Then, the clusters connect with each other to form stable basic hydrate, and the connection among the clusters in this step leads to the formation of the linked cavities, which are also called the small cavities [32]. It should be pointed out that basic hydrate is stoichiometric, and for the hydrate with a specific structure (structure I, etc.), the ethylene-to-water ratio of molecular numbers in basic hydrate (λ_2) is a fixed constant (3/23 for structure I hydrate) [39]. This step can be illustrated as [32]:

$$\lambda_2 \cdot C_2H_4 + H_2O \rightarrow H_2O \cdot C_2H_{4\lambda_2} \quad (6)$$

The second step is that the molecules (S), which are smaller than the small cavities, are adsorbed into the empty small cavities of basic hydrate [32]. In this step, hydrate converts from basic hydrate to final hydrate:

$$H_2O \cdot C_2H_{4\lambda_2} + \lambda_1 \cdot \theta \cdot S \rightarrow H_2O \cdot C_2H_{4\lambda_2} \cdot S_{\lambda_1 \cdot \theta} \quad (7)$$

where λ_1 is the ratio of the small cavity-to-water molecule numbers in basic hydrate (1/23 for structure I hydrate) and θ is the occupation fraction (%) of the small cavities filled by small gas molecules. It should be pointed out that, since ethylene molecules are larger than the small cavities of hydrate, the second step does not occur in the formation of ethylene hydrate, which is different from the prediction models mentioned in Section 4.1 [15,46–49]. When the basic hydrate formation shown in Equation (6) reaches equilibrium [15]:

$$\mu_{C_2H_4} = \mu^0_{C_2H_4} + RT \ln f_{C_2H_4} \quad (8)$$

$$\mu^0_B - \mu_w - \lambda_2 \mu^0_{C_2H_4} = \lambda_2 RT \ln f^0_{C_2H_4} \quad (9)$$

where μ^0_B is the chemical potential of the basic hydrate, $\mu_{C_2H_4}$ and μ_w are the chemical potentials of C_2H_4 and water, respectively, $\mu^0_{C_2H_4}$ is the chemical potential of the C_2H_4 at ideal gas state, $f_{C_2H_4}$ is the fugacity of the C_2H_4 under the experimental condition and is calculated by Patel-Teja EOS [44] and $f^0_{C_2H_4}$ is the fugacity of the C_2H_4 in the basic hydrate under the experimental condition. Since the second step does not occur in the formation of ethylene hydrate, the basic hydrate is the final hydrate, so that the chemical potential of the final hydrate (μ_B) can be calculated as follows [39]:

$$\mu_B = \mu^0_B \quad (10)$$

The change of the chemical potential during the hydrate formation ($\Delta\mu$) is the difference between the final chemical potential and the initial chemical potential ($\mu_B - \mu_{initial}$) [15]:

$$\mu_{initial} = \mu_w + \lambda_2 \mu_{C_2H_4} \quad (11)$$

Combining Equations (8)–(11):

$$\Delta\mu = \mu_B - \mu_{initial} = RT\lambda_2 \ln(f^0_{C_2H_4}/f_{C_2H_4}) \quad (12)$$

$f^0_{C_2H_4}$ is calculated as follows [39]:

$$f^0_{C_2H_4} = f^0_T(T)\cdot \exp\left(\frac{\beta P}{T}\right)\cdot \alpha_w^{-1/\lambda_2} \quad (13)$$

where β is a structure parameter (0.4242 K/bar for structure I hydrate) and α_w is the activity of the water in the liquid phase. The host lattice relaxation, guest–host interactions and the quantum nature of guest behavior are introduced into the models by introducing an Antoine-type equation $f^0_T(T)$ into the calculation of $f^0_{C_2H_4}$, and the Antoine parameters are fitted using the pure gas hydrate formation data for a particular structure only [39]:

$$f^0_T(T) = A' \exp[B'/(T - C')] \quad (14)$$

where A′ is 4.8418 × 10^{11} bar, B′ is −5597.59 K and C′ is 51.8 K [39]. SLS does not form hydrate, and its thermodynamic effect on hydrate formation in the model calculation mainly manifests as its effects on α_w. The SLS solution is an electrolyte solution, the α_w is calculated by the Modified PT EOS [44,50] and the calculation process is shown in the Supplementary Materials. Since the ionic diameter and polarizability of the anion of SLS used for the calculation of α_w have not been reported, they (23.87 Å and 35.92 $Å^3$) were fitted using the experimental data in Section 4.1; the fitting process is shown in the Supplementary Materials. The parameters used for the calcuation of $f^0_{C_2H_4}$ is shown in Table S4 in the Supplementary Materials.

$P_{eq,Cal}$ is the P_{eq} in the model calculation. Whether hydrate can be formed can be determined directly according to $\Delta\mu$. Because $\Delta\mu$ is negative when the pressure is higher than the $P_{eq,Cal}$, $\Delta\mu$ is positive when the pressure is lower than $P_{eq,Cal}$, and $\Delta\mu$ equals to zero when the pressure equals to $P_{eq,Cal}$ [15]. It should be pointed out that $P_{eq,Cal}$ is unique when temperature and phase compositions are all determined [15]. Since $P_{eq,Cal}$ could be an irrational number, it is not certain whether $P_{eq,Cal}$ can be determined directly by a trial-and-error method. However, the range of $P_{eq,Cal}$ can be easily determined, because $\Delta\mu$ increases monotonously with the decrease of pressure [15]. The flow chart of the calculation of $P_{eq,Cal}$ is shown in Figure 2. The iterative computation was edited by Visual basic 6.0 and can also be edited by the software which can be used in iterative computation.

In Figure 2, w_p is the concentration of the promoter (SLS) in the liquid phase and P_u is the uncertainly of $P_{eq,Cal}$ and is set at 0.001 MPa in this work, because P_u should be smaller than the uncertainty of the experimental P_{eq} (0.01 MPa in Section 4.1).

When $\Delta\mu$ is positive under $P - 0.5P_u$ and negative under $P + 0.5P_u$, which means that $P - 0.5P_u$ is lower than $P_{eq,Cal}$ and $P + 0.5P_u$ is higher than $P_{eq,Cal}$, the difference between P and $P_{eq,Cal}$ is smaller than P_u, which means that P can be regarded as $P_{eq,Cal}$ and the accuracy meets the requirement of the model calculation. When $\Delta\mu$ is positive under $P - 0.5P_u$ as well as $P + 0.5P_u$, P is lower than $P_{eq,Cal}$ and the difference between P and $P_{eq,Cal}$ can be larger than P_u. When $\Delta\mu$ is negative under $P - 0.5P_u$ as well as $P + 0.5P_u$, P is higher than $P_{eq,Cal}$ and the difference between P and $P_{eq,Cal}$ can be larger than P_u. It should be pointed out that if $\Delta\mu$ is negative under $P - 0.5P_u$ but positive under $P + 0.5P_u$ (which never happened in this work), which means that $P_{eq,Cal}$ is smaller than $P - 0.5P_u$ but is higher than $P + 0.5P_u$, which is contrary to reality, then the calculation would end and the model would be rechecked.

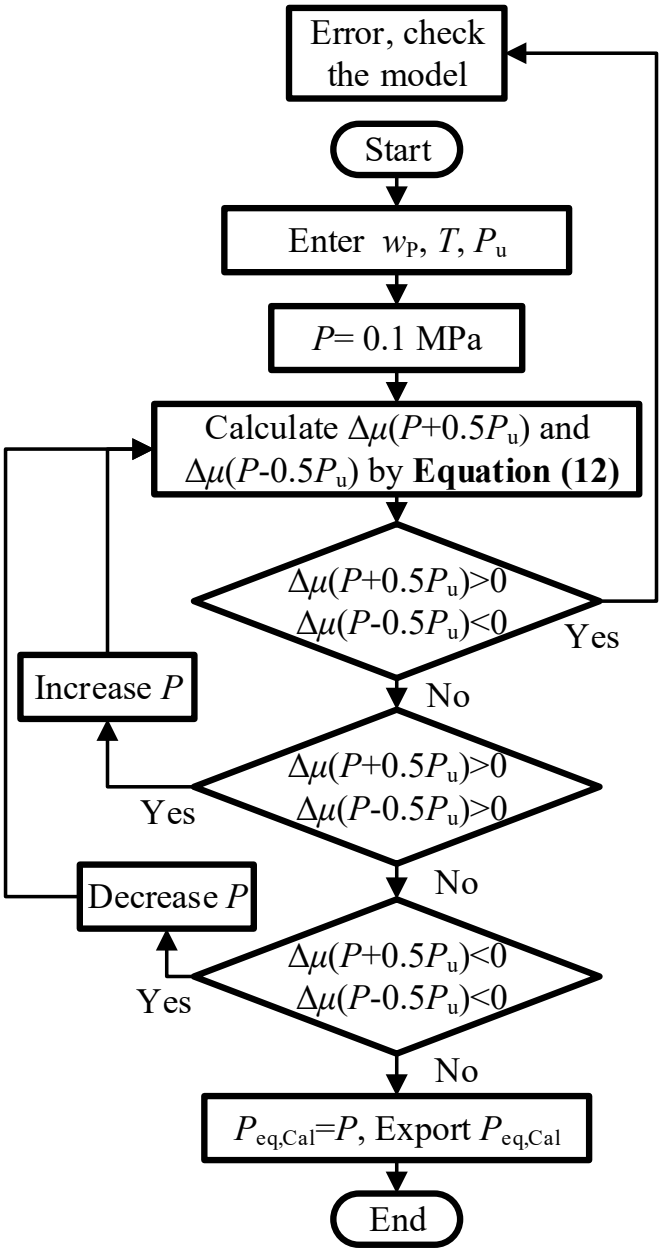

Figure 2. Schematic diagram of the calculation of $P_{eq,Cal}$.

The relative deviation (*RD*), maximum relative deviation (*MRD*), average relative deviation (*ARD*) and goodness of fit (*GF*) are used to describe the deviation between $P_{eq,Cal}$ and $P_{eq,Exp}$:

$$RD = \left(P_{eq,Exp} - P_{eq,Cal}\right)/P_{eq,Exp}\cdot 100\% \tag{15}$$

$$MRD = \max\left(\left|\frac{P_{eq,Exp,ii} - P_{eq,Cal,ii}}{P_{eq,Exp,ii}}\right|\right)\cdot 100\% \tag{16}$$

$$ARD = \sum_{ii}^{n}\left|\frac{P_{eq,Exp,ii} - P_{eq,Cal,ii}}{P_{eq,Exp,ii}}\right|/n\cdot 100\% \tag{17}$$

$$GF = 1 - \frac{\sum_{ii}^{nn}\left(P_{eq,Exp,ii} - P_{eq,Cal,ii}\right)^2}{\sum_{ii}^{nn}\left(P_{eq,Exp,ii} - \sum_{ii}^{nn} P_{eq,Exp,ii}/nn\right)^2} \tag{18}$$

where n is the number of the experiments in Section 4.1, nn denotes the number of the experimental temperatures in Section 4.1 and ii denotes the serial number. Smaller *RD*, *MRD* and *ARD* indicate a better prediction accuracy of the model. A value of *GF* close to 1 means that the model can predict the effect of temperature on P_{eq} accurately.

The initial related deviation (DRS_0) is used to quantitatively described the initial THFDF and the difference between the initial state of the hydrate formation and the state of thermodynamic phase equilibrium. The final related deviation (DRS_{end}) is used to quantitatively described the THFDF at the end of the hydrate formation and the difference between the final state of the hydrate formation and the state of thermodynamic phase equilibrium:

$$DRS_0 = (P_f - P_{eq,0})/P_{eq,0} \times 100\% \quad (19)$$

$$DRS_{end} = (P_f - P_{eq,end})/P_{eq,end} \times 100\% \quad (20)$$

where $P_{eq,0}$ and $P_{eq,end}$ are the thermodynamic phase equilibrium pressures under the initial condition of the hydrate formation and the condition the end of the hydrate formation, respectively, which are calculated using the method shown in Figure 2. Since the gas composition (pure ethylene), pressure and temperature were all kept constant in each individual hydrate formation process, the difference between $P_{eq,0}$ and $P_{eq,end}$ is caused by the change in the SLS concentration in liquid phase. The SLS concentration in the liquid phase at the end of the hydrate formation ($w_{p,end}$) is calculated using the amount of the water in the hydrate phase ($N_{w,h}$), and N_d comes from experimental data. Ethylene molecules only occupy the large cavities of hydrate, so that no ethylene molecule is in the small cavities. The $N_{w,h}$, $w_{p,end}$ and R_{WH} can be calculated as:

$$N_{w,h} = N_d/\lambda_2 \quad (21)$$

$$w_{p,end} = m_{SLS}/(m_0 - M_w \cdot N_{w,h}) \times 100\% \quad (22)$$

$$R_{WH} = N_{w,h}/[(m_0 - m_{SLS})/M_w] \times 100\% \quad (23)$$

where m_{SLS} is the mass of the SLS in the solution and m_0 is the mass of the SLS solution injected into the crystallizer. SLS does not form hydrate and rarely goes into gas phase, so that m_{SLS} is assumed constant during the hydrate formation process.

4. Results and Discussion

4.1. The Thermodynamic Effect of SLS on Ethylene Hydrate Formation

The thermodynamic effect of SLS on hydrate formation manifests as the effect of SLS on the P_{eq}. As discussed previously, the w_p increases with the increase in R_{WH}, and SLS might have a significant thermodynamic effect on hydrate formation when R_{WH} is high [30]. The surfactants used in hydrate formation should not have a significant negative thermodynamic effect on hydrate formation. The thermodynamic effect of SLS on hydrate formation was investigated in this section to ensure that SLS meets the thermodynamic requirement of the surfactants, as well as to lay a foundation for the investigation in Section 4.3.

In the previous research [7], the maximum R_{WH} in hydrate formation in the presence of SDS can be as high as 90%. The w_p is about 10 times as high as $w_{p,0}$ when R_{WH} is 90% and about twice the $w_{p,0}$ when R_{WH} is 50%. Since the $w_{p,0}$ in Section 4.3 is not higher than 0.5 mass%, the SLS concentrations in the liquid phase were set at 1.0 mass% (=0.5 mass% × 2) and 5.0 mass% (=0.5 mass% × 10). The P_{eq} of ethylene gas with different liquids at different temperatures are shown in Table 1. The uncertainties of the experimental data and calculated data are ±0.01 MPa and ±0.001 MPa, respectively.

Table 1. The experimental and calculated thermodynamic equilibrium hydrate formation pressures.

T (K)	Pure Water			1.0 mass% SLS			5.0 mass% SLS		
	$P_{eq,Exp}$ (MPa)	$P_{eq,Cal}$ (MPa)	*RD* (%)	$P_{eq,Exp}$ (MPa)	$P_{eq,Cal}$ (MPa)	*RD* (%)	$P_{eq,Exp}$ (MPa)	$P_{eq,Cal}$ (MPa)	*RD* (%)
275.15	0.68	0.674	0.9	0.69	0.680	1.4	0.71	0.704	0.8
276.65	0.82	0.806	1.7	0.82	0.813	0.9	0.85	0.842	0.9
278.15	0.99	0.963	2.7	1.02	0.972	4.7	1.04	1.007	3.2
279.65	1.17	1.152	1.5	1.19	1.162	2.4	1.23	1.206	2.0
281.15	1.38	1.379	0.1	1.41	1.392	1.3	1.46	1.445	1.0
282.65	1.68	1.655	1.5	1.70	1.670	1.8	1.75	1.737	0.7

The experimental data in Table 1 shows that $P_{eq,Exp}$ increases with the increase in w_p, which confirms the hypotheses that SLS has a negative thermodynamic effect on hydrate formation and the negative thermodynamic effect increases with the increase in the w_p. However, the increase in $P_{eq,Exp}$ caused by SLS are very small in Table 1, and the difference between the $P_{eq,Exp}$ of the pure water system and the $P_{eq,Exp}$ of the 1.0 mass% SLS system at the same temperature is smaller than 0.03 MPa, while the difference between the $P_{eq,Exp}$ of the pure water system and the $P_{eq,Exp}$ of the 5.0 mass% SLS system at the same temperature is smaller than 0.08 MPa. The increases in $P_{eq,Exp}$ caused by SLS are smaller than those caused by other salts (sodium chloride etc. [51]) and hydrate inhibitors (methanol etc. [27]) with the same mass fraction. Since the $w_{p,0}$ is not higher than 0.5 mass% when SLS is used as a surfactant, the SLS concentration in liquid phase is normally not higher than 5.0 mass% during the hydrate formation process. For this reason, the hypotheses that the negative thermodynamic effect of SLS on hydrate formation is significant when R_{WH} is very high is not true.

The prediction data ($P_{eq,Cal}$) are provided in Table 1 for verification. The model predicts well the effects of temperature and the SLS concentration in the liquid phase on the P_{eq}, the *ARD* of all the data in Table 1 is 1.6%, the *MRD* of all the data in Table 1 is 4.7% and the *GF* for the three curves of the P_{eq} vs. temperature of the pure water system, 1.0 mass% SLS system and 5.0 mass% SLS system are all higher than 0.994. The performance of this model is as good as the performances of the models in the literature on predicting the P_{eq} under the experimental conditions in their own works (*ARD* is 2.6% for the fluid catalytic cracking (FCC) dry gas + Poly (sodium 4-styrenesulfonate) (PSS) solution/pure water system [15], 2.56% for the N_2+CO_2+water system [46], 0.66% for the CH_4+CO_2+H_2S+N_2+methanol solution system [47], 5.8% for the H_2S(liquid)+water system [48], 1.1% for the H_2S(gas)+water system [48] and 1.43% for the CH_4+water system [49]. *GF* is 0.994 for the N_2+CO_2+water system [46] and is higher than 0.978 for the FCC dry gas + PSS solution/pure water system [15]).

According to the results of Section 4.1, SLS meets the thermodynamic requirement of the surfactants used in hydrate formation, and the model proposed in this paper can accurately describe the thermodynamic effect of SLS on hydrate formation.

4.2. The Interfacial Tension between the Ethylene Gas and SLS Solution

Since the gas–liquid interfacial tension is necessary for the discussion on the kinetic effect of SLS on hydrate formation in Section 4.3, the interfacial tension of the ethylene–SLS solution was measured and is shown in Figure 3. The average values of the data are shown as symbols, and the uncertainties of data caused by repeated experiments are shown as error bars. Since the uncertainties of the data are too small compared with the average data, the error bars are not distinct in Figure 3. The data of each individual experiment are shown in Tables S1 and S2 in Supplementary Materials.

As is shown in Figure 3, the interfacial tension is effectively decreased by using SLS. The gas–liquid interfacial tensions of water system are all higher 73 mN·m^{-1}, whereas those of the SLS solution systems are all lower than 65 mN·m^{-1}.

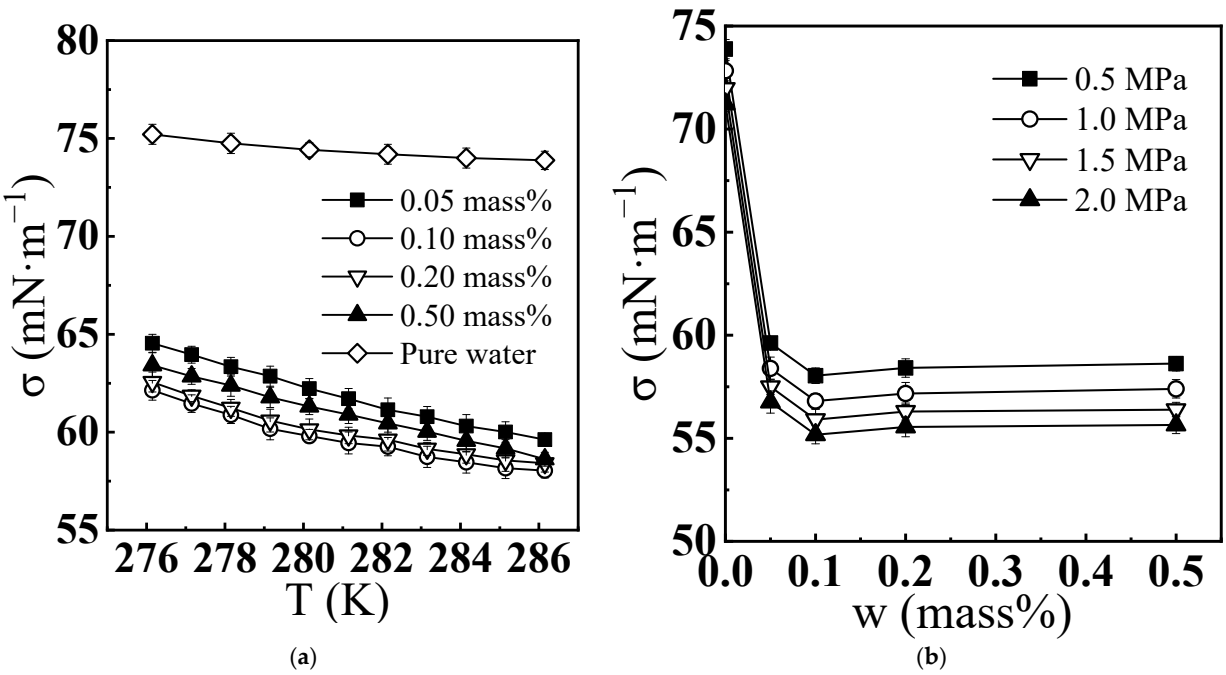

Figure 3. The interfacial tensions (σ mN·m^{-1}) between ethylene and (**a**) different liquids at different temperatures under 0.5 MPa; (**b**) different liquids under different pressures at 286.15 K.

In Figure 3, an increase in either temperature or pressure leads to a decrease in the interfacial tension, and this phenomenon is also found in the studies on the interfacial tensions between coal seam gas and TBAB solution [52], as well as ethylene gas and SDS solution [53].

In Figure 3b, as the SLS concentration increases, the interfacial tension between ethylene gas and liquid phase decreases at first then slightly increases. The inflection point in the above relationship between SLS concentration and the interfacial tension is at 0.1 mass% SLS, which indicates that the critical micelle concentration (CMC) of SLS is about 0.1 mass%. The relationship between the concentration of the surfactant in liquid phase and the gas–liquid interfacial tension, which is the same as that between the SLS concentration and the interfacial tension in this work, can also be found in the studies on the interfacial tensions between FCC dry gas and PSS solution [15], as well as air and n-octyl-β-D-glucopyranoside solution [54].

Taking the foaming ability, resource utilization, environmental protection and the performance of SLS on decreasing gas–liquid interfacial tension into consideration, SLS is a surfactant with good potential in hydrate formation.

4.3. The Kinetic Effect of SLS on Ethylene Hydrate Formation

The kinetic effect of SLS on hydrate formation, which mainly manifests as the effects of SLS on the hydrate formation rate (r_R) and the conversion rate of the water into hydrate at the end of the hydrate formation ($R_{WH,end}$) in the hydrate formation controlled by mass transfer, was investigated by investigating the effects of $w_{p,0}$ and pressure on the final state of ethylene formation, as well as on the r_R at different stages in the process of hydrate formation in this section.

The changes of temperature, pressure and gas composition can lead to significant changes in the THFDF, and the effect of the change in THFDF can override the thermodynamic and kinetic effects of SLS on hydrate formation [15]. For the above reasons, pure ethylene gas was used as the experimental gas so that the gas composition did not change along with hydrate formation, and the temperature as well as the pressure was kept constant in each individual experiment in this work.

4.3.1. The Effect of the Initial SLS Concentration in the Liquid Phase on Ethylene Hydrate Formation

SLS can affect hydrate formation by affecting the properties of liquid phase (such as the gas–liquid interfacial tension) like other surfactants (such as SDS [53] and Poly (sodium 4-styrenesulfonate) [15]). Since the gas–liquid interfacial tension is affected by the SLS concentration in liquid, the effect of the $w_{p,0}$ on the ethylene hydrate formation was investigated in this section. The P_f and T_f were set at 278.15 K under 1.24 MPa to ensure a strong THFDF. The average data and the uncertainties of the average data are presented in Table 2. The data of each individual hydrate formation experiment are shown in Table S3 in Supplementary Materials. The difference between $P_{eq,0}$ and $P_{eq,end}$ represents the change in THFDF during hydrate formation. DRS_0 and DRS_{end} represent the THFDF at the initial stage and final stage of hydrate formation, respectively.

Table 2. The effect of the $w_{p,0}$ on the final state of ethylene hydrate formation.

$w_{p,0}$ (mass%)	$P_{eq,0}$ (MPa)	DRS_0 (%)	$P_{eq,end}$ (MPa)		DRS_{end} (%)		*GSCHS* (NL/L)		$R_{WH,end}$ (%)		$w_{p,end}$ (mass%)	
			$\overline{Data}$	$Data_u$ (±)	$\overline{Data}$	$Data_u$ (±)	$\overline{Data}$	$Data_u$ (±)	$\overline{Data}$	$Data_u$ (±)	$\overline{Data}$	$Data_u$ (±)
0.00	0.963	28.8	0.963	0.000	28.8	0.0	92.7	2.7	57.6	1.6	0.00	0
0.05	0.964	28.6	0.965	0.000	28.5	0.0	112.9	3.5	70.1	2.1	0.17	0.01
0.10	0.964	28.6	0.967	0.000	28.2	0.0	124.0	3.4	77.0	2.1	0.44	0.04
0.20	0.965	28.5	0.970	0.001	27.8	0.1	121.6	2.5	75.6	1.5	0.82	0.05
0.50	0.967	28.2	0.979	0.001	26.7	0.2	117.4	2.1	73.2	1.3	1.85	0.09

In each experiment in Table 2, DRS_0 and DRS_{end} have no significant difference, which means that the decrease in THFDF during hydrate formation was very small. This is because the difference between $P_{eq,0}$ and $P_{eq,end}$ was very small in each experiment. Since pressure, temperature and gas composition kept constant in each individual experiment, the difference between $P_{eq,0}$ and $P_{eq,end}$ was determined by the change in the liquid composition during hydrate formation. Since the increase in the w_p during hydrate formation was not significant (smaller than 1.50 mass% SLS) and the thermodynamic effect of SLS on hydrate formation is small, the difference between $P_{eq,0}$ and $P_{eq,end}$ was small.

Based on the data in Table 2, it was the hydrate shell effect (ethylene gas and water were separated by hydrate, so that they could not contact with each other) [55] rather than the thermodynamic phase equilibrium that stopped the hydrate formations in this section. DRS_{end} is far higher than 0%, which indicates that THFDF was still strong at the end of the hydrate formation. $R_{WH,end}$ is far less than 100%, since ethylene was oversupplied in each experiment, and the end of the hydrate formation was not caused by the lack of water nor by the lack of ethylene.

In Table 2, the presence of SLS makes little difference in DRS_0, whereas it significantly increases $R_{WH,end}$: $R_{WH,end}$ is 57.6 ± 1.6% in the hydrate formation using pure water, whereas it is higher than 70.0% in the hydrate formations using SLS solutions, which indicates the increased $R_{WH,end}$ is from the kinetic effect of SLS on ethylene hydrate formation. As discussed previously, the hydrate shell effect ends hydrate formation before the THFDF decreases to zero, and the hydrate shell effect is caused by the low mass transfer rate (which makes the r_R in liquid phase much lower than the r_R in the areas that are near the gas–liquid interface, so that the gas–liquid interface is covered by hydrate before all the water converts into hydrate) and the aggregation of hydrate particles (which makes water wrapped by hydrate) [56]. SLS increases the mass transfer rate [16], which effectively reduces the difference in the r_R in different areas [55]. SLS adsorbs on the surface of hydrate and decreases the liquid force between adjacent hydrate particles [17], which effectively prevents the aggregation of hydrate particles [55]. For the above reasons, SLS can effectively reduce the hydrate shell effect.

In Table 2, as $w_{p,0}$ increases, $R_{WH,end}$ increases at first then slightly decreases, and the inflection point in the above relationship between $w_{p,0}$ and $R_{WH,end}$ is at 0.10 mass%.

This may be caused by the change in the gas–liquid interfacial tension, which is caused by the change in $w_{p,0}$. SLS increases $R_{WH,end}$ by reducing the hydrate shell effect, which is reduced by increasing the mass transfer rate and preventing the aggregation of hydrate particles. Since the SLS increases the mass transfer rate and decreases the liquid force between adjacent hydrate particles by decreasing the gas–liquid interfacial tension [55], the increase of $R_{WH,end}$ is affected by the gas–liquid interfacial tension. Since the w_p increases with the increase in the R_{WH} in hydrate formation process and the lowest gas–liquid interfacial tension is achieved at 0.1 mass% SLS, the gas–liquid interfacial tensions of the 0.2 mass% SLS system and the 0.5 mass% SLS system were higher than the gas–liquid interfacial tension 0.1 mass% SLS system during the whole hydrate formation process. In most stages of hydrate formation, the gas–liquid interfacial tension of the 0.05 mass% SLS system was lower than those of the other SLS solutions. Though the increases in R_{WH} led to the decrease in the gas–liquid interfacial tension of the 0.05 mass% SLS system, which caused the increase of R_{WH}, the increase in R_{WH} led to the increase in the mass transfer resistance and the decrease in the fluidity of the hydrate slurry at the same time, which overrides the effect of the decrease in the gas–liquid interfacial tension. Compared with the difference between the $R_{WH,end}$ of the water system and the $R_{WH,end}$ of the SLS solution system, the differences among the $R_{WH,end}$ of the different SLS solution systems are not significant, which may be because the gas–liquid interfacial tensions of the SLS solutions in Table 2 are close, which can be seen from either Figure 3 or the data of the gas–liquid interfacial tensions in the Supplementary Materials. In Table 2, *GSCHS* is proportional to $R_{WH,end}$, because ethylene is stored by forming hydrate.

Figure 4 represents the average kinetic data of the hydrate formation with different $w_{p,0}$ at 278.15 K under 1.24 MPa (calculated by Equation (4)). The uncertainties of the kinetic data for the three repeated experiments are shown as error bars (calculated by Equation (5)). The effect of $w_{p,0}$ on the relationship between R_{WH} and time is shown in Figure 4a. Since the introduction periods of hydrate formations were not obvious under the operating conditions in this work, the time zero in Figure 4a is set at the time the experiment begins. The effect of $w_{p,0}$ on the r_R at different stages in the process of hydrate formation is shown in Figure 4b and the data are from the R_{WH} of 5%. The temperature inside the crystallizer normally slightly fluctuated when hydrate started forming, and it returned to the experimental temperature and was kept constant before R_{WH} increased to 5%.

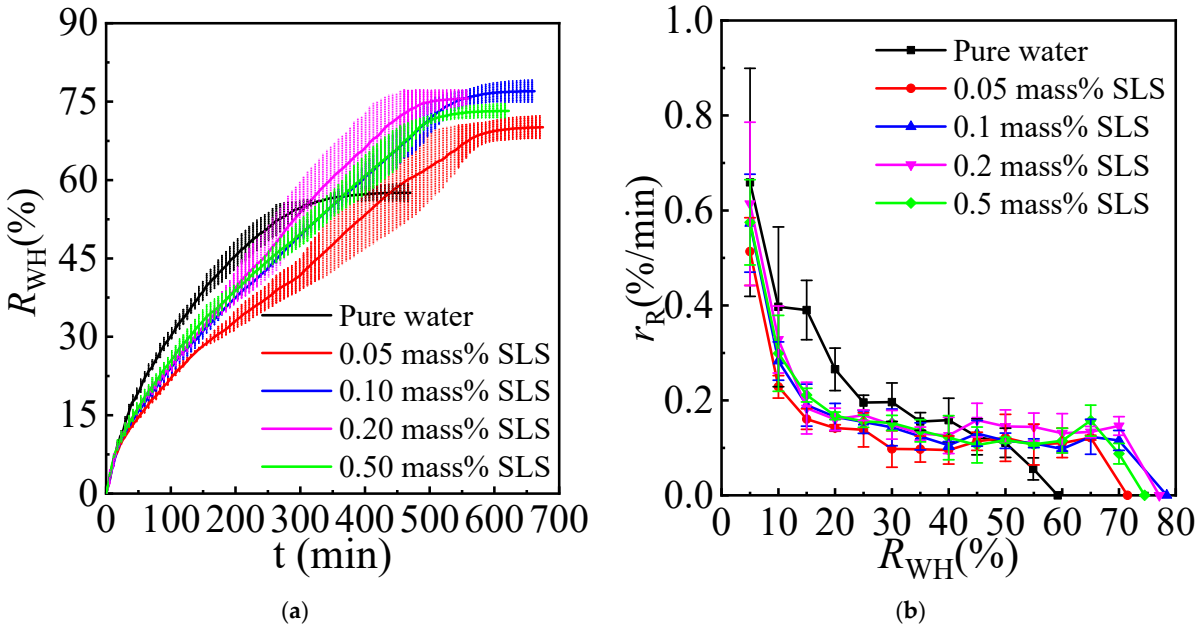

Figure 4. The kinetic data of the hydrate formation with different $w_{p,0}$ at 278.15 K under 1.24 MPa: (**a**) R_{WH} vs. time; (**b**) r_R vs. R_{WH}.

In Figure 4a, the hydrate formation in the presence of SLS is slower than the hydrate formation using pure water at first, but the hydrate in the presence of SLS still forms after the hydrate formation using pure water ends. This may be caused by the adsorption of the anion of SLS (LS^-) on the hydrate surface [57,58] and the decrease in the liquid force between adjacent hydrate particles caused by SLS [17,55]. The adsorption of LS^- on the hydrate surface decelerates the growth of hydrate, which causes a negative effect on hydrate formation [57,58]. However, the adsorption of LS^- on the hydrate surface prevents the agglomeration of hydrate particles, which causes a positive effect on hydrate formation at the same time [17,55]. The adsorption of LS^- on the hydrate surface and the decrease in the liquid force between adjacent hydrate particles effectively reduces the hydrate shell effect [17,55], which ensures the hydrate in the presence of SLS still forms after the hydrate formation using pure water ends [17].

In Figure 4a,b, the r_R in the hydrate formation using SLS solution does not decreases with the increase in $w_{p,0}$, which indicates that the negative effect of SLS on r_R does not increases with the increase of $w_{p,0}$ in the experimental range. The r_R in the hydrate formation using the 0.2 mass% SLS solution is slightly faster than those of the hydrate formations using the other SLS solutions, whereas the formation rates of the hydrate formation using the 0.1 mass% SLS solution and 0.5 mass% SLS solution show little difference. That indicates that, in a specific SLS concentration range, increasing $w_{p,0}$ can increase the positive effect of SLS on the r_R, and this trend is also found in the hydrate formations of the CH_4+ lithium dodecyl sulfate solution system [59] and CH_4+ dodecylbenzene sulfonic acid solution system [59].

In Figure 4b, the r_R in the hydrate formation using pure water is faster than the r_R in the hydrate formation using the SLS solution when R_{WH} is lower than 30%, whereas it is slower than the r_R in the hydrate formation using the SLS solution when R_{WH} is higher than 55%.

The r_R in the hydrate formation using pure water decreases with the increase in R_{WH} whereas the r_R in the hydrate formations in the presence of SLS rarely changes as R_{WH} increases from 25% to 65%, which indicates that the r_R is determined by mass transfer resistance and the mass transfer resistance in the hydrate formation using SLS solution rarely increases as R_{WH} increases from 25% to 65%, whereas the mass transfer resistance in the hydrate formation using pure water significantly increases continuously with the increase of R_{WH}.

The r_R in the hydrate formation using 0.05 mass% SLS solution significantly decreases with the increase in R_{WH} when R_{WH} is higher than 65%, whereas the r_R in the hydrate formations using the other SLS solutions significantly decrease with the increase in R_{WH} when R_{WH} is higher than 70%. That means that the effect of SLS on reducing the hydrate shell effect is not unlimited; when R_{WH} reaches a specific value, SLS cannot promote the hydrate formation any longer. In this paper, the specific value of R_{WH} is about 65% for the hydrate using the 0.05 mass% SLS solution and is about 70% for the hydrate using the other SLS solutions.

4.3.2. The Effect of Pressure on Ethylene Hydrate Formation

The effect of the THFDF (which is proportional to pressure) on the hydrate formation in the presence of SLS was investigated by investigating the effect of pressure on ethylene hydrate formation in the presence of SLS, and the corresponding experimental data are presented in Table 3. The data of each individual hydrate formation experiment are shown in Table S3 in the Supplementary Materials. The $w_{p,0}$ was set at 0.10 mass%, and the temperature was set at 278.15 K to ensure a strong THFDF.

In Table 3, the difference between DRS_0 and DRS_{end} as well as the difference between $P_{eq,0}$ and $P_{eq,end}$ is small under each pressure, which indicates that the decrease in THFDF during the hydrate formation is very small regardless of whether the pressure is high. The reasons for those little differences are the little thermodynamic effect of SLS on hydrate formation and the difference between $w_{p,0}$ and $w_{p,end}$, which has been discussed in

Section 4.3.1. Since DRS_{end} values are all far higher than 0% and $R_{WH,end}$ values are all far less than 100% in this section, the hydrate formations were stopped by mass transfer resistance, which are the same as those in Section 4.3.1.

Table 3. The effect of pressure on the final state of ethylene hydrate formation.

P (MPa)	$P_{eq,0}$ (MPa)	DRS_0 (%)	$P_{eq,end}$ (MPa)		DRS_{end} (%)		*GSCHS* (NL/L)		$R_{WH,end}$ (%)		$w_{p,end}$ (mass%)	
			$\overline{Data}$	$Data_u$ (±)	$\overline{Data}$	$Data_u$ (±)	$\overline{Data}$	$Data_u$ (±)	$\overline{Data}$	$Data_u$ (±)	$\overline{Data}$	$Data_u$ (±)
1.12	0.964	16.2	0.966	0.000	15.9	0.0	110.1	2.4	68.4	1.5	0.32	0.02
1.24	0.964	28.6	0.967	0.000	28.2	0.0	124.0	3.4	77.0	2.1	0.44	0.04
1.49	0.964	54.6	0.967	0.001	54.0	0.1	128.1	3.3	79.6	2.0	0.49	0.05
2.00	0.964	107.5	0.967	0.000	106.8	0.0	122.4	2.9	76.1	1.8	0.42	0.03

In Table 3, the $R_{WH,end}$ in the hydrate formation under 1.12 MPa (64.8 ± 1.5%) is lower than those in the hydrate formations under the other pressures, whereas the $R_{WH,end}$ values in the hydrate formations under the other three pressure have no significant difference. The $R_{WH,end}$ in the hydrate formation under 2.00 MPa is slightly lower than $R_{WH,end}$ in the hydrate formation under 1.49 MPa. The above indicates that the increase in the pressure leads to an increase in the $R_{WH,end}$ when the pressure is lower than 1.49 MPa, whereas the increase in pressure leads to a slight decrease in the $R_{WH,end}$ when the pressure is higher than 1.49 MPa. The above relationship between the $R_{WH,end}$ and pressure may be caused by the effects of THFDF and the mass transfer. The increase in pressure leads to the the increase of THFDF and the mass transfer force, and that leads to the increase of the r_R and $R_{WH,end}$; however, when pressure is higher than a specific value, as pressure increases, the increase in the mass transfer rate cannot keep up with the increase of the r_R, which leads to the increase in the hydrate shell effect and leads to the decrease of the $R_{WH,end}$ [60].

In Table 3, *GSCHS* and $w_{p,end}$ increase with the increase in pressure and then decreases, and their highest values are achieved under 1.49 MPa. This is because ethylene is stored by forming hydrate and $w_{p,end}$ is inversely proportional to the amount of residual water, which makes *GSCHS* and $w_{p,end}$ proportional to $R_{WH,end}$.

Figure 5 represents the kinetic data of the hydrate formation under different pressures at 278.15 K with the $w_{p,0}$ of 0.10 mass%. In Figure 5a,b, a higher pressure leads to a higher r_R, which is because a higher pressure leads to a higher THFDF. However, when the r_R is very high, the mass transfer rate cannot keep up with the r_R, which increases the hydrate shell effect, and that leads to a low $R_{WH,end}$ [60]. For the above reason, the r_R in the hydrate formation under 2.00 MPa is faster than the r_R in the hydrate formations under the other pressures, but the $R_{WH,end}$ in the hydrate formation under 2.00 MPa is smaller than $R_{WH,end}$ in the hydrate formation under 1.49 MPa.

Though the THFDF values are proportional to pressure and do not significantly change along with the hydrate formation in each individual experiment, in Figure 5b, the differences among the r_R under different pressures grow smaller as R_{WH} increases from 5% to 30%, which indicates that the mass transfer resistance increases as R_{WH} increases from 5% to 30%. The r_R under different pressures have no significant difference when R_{WH} is between 30% and 65%, which indicates that the hydrate formations are controlled by mass transfer and the mass transfer resistance does not significant increases as R_{WH} increases from 30% to 65%. The steady r_R makes the hydrate process easier to control, which indicates that SLS has a good potential in the application of hydrate-based technologies.

The r_R in the hydrate formation under 1.12 MPa significantly decreases with the increase in R_{WH} when R_{WH} is higher than 65%, whereas the r_R in the hydrate formations under the other pressures significantly decrease with the increase in R_{WH} when R_{WH} is higher than 70%. The above indicates that when the pressure is higher than a specific value, r_R can no longer be kept by increasing the pressure.

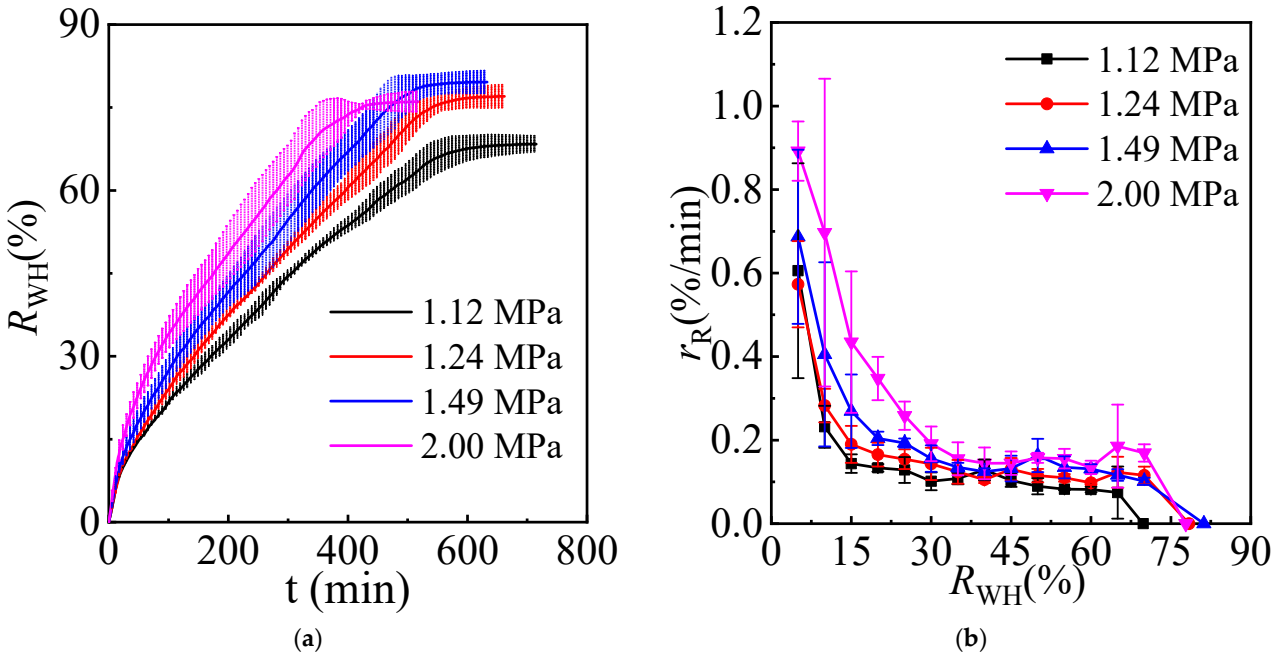

Figure 5. The kinetic data of hydrate formation under different pressure at 278.15 K with the $w_{p,0}$ of 0.10 mass%: (**a**) R_{WH} vs. time; (**b**) r_R vs. R_{WH}.

5. Conclusions

How to increase R_{WH} through a cheap method is the key concern in the advances in gas hydrate technologies, and SLS shows good potential to increase R_{WH}. The thermodynamic effect of SLS on hydrate formation was experimentally investigated and quantitatively described for the first time in this paper. The effects of the initial SLS concentration and pressure on the hydrate formation at different stages of the hydrate formation process was experimentally investigated for the first time.

A new model was proposed to predict the P_{eq}. Based on the model, the thermodynamic effect of SLS on the hydrate formation, the THFDF and the difference between the state of hydrate formation and thermodynamic phase equilibrium can be quantitatively described. The $P_{eq,Cal}$ matches the $P_{eq,Exp}$ well, the *ARD* is 1.6% and the *MRD* is 4.7%. The *GF* of the P_{eq} vs. temperature of the pure water system, 1.0 mass% SLS system and 5.0 mass% SLS system are all higher than 0.994.

The gas–liquid interfacial tension was effectively decreased by using SLS. SLS had no significant negative thermodynamic effect on hydrate formation. SLS increased the $R_{WH,end}$: $R_{WH,end}$ was increased from 57.6 ± 1.6% to higher than 70.0% by using SLS, and the highest $R_{WH,end}$ (77.0 ± 2.1%) was achieved when $w_{p,0}$ was 0.1 mass%.

The formation rate of the hydrate in the presence of SLS did not significantly change as R_{WH} increased from 35% to 65%. The effect of increasing pressure on an increasing hydrate formation rate decreased with the increase in R_{WH}. When R_{WH} was higher than 30%, the hydrate formation was controlled by mass transfer and increasing pressure could not significantly increase the hydrate formation rate.

Since SLS increases $R_{WH,end}$ and steadies the hydrate formation rate in a large R_{WH} range, it has good potential in the application of hydrate-based technologies.

Supplementary Materials: The following are available online at https://www.mdpi.com/article/10.3390/en14113291/s1, Table S1: The interfacial tensions between ethylene gas and different liquids at different temperatures under 0.5 MPa, Table S2: The interfacial tensions between ethylene gas and different liquids under different pressures at 286.15 K, Table S3: The effect of SLS on hydrate formation, Table S4: The parameters for the calculation of f^0.

Author Contributions: Conceptualization, Y.W.; methodology, Y.W.; software, Q.S.; validation, L.Y., L.W., Z.H. and Y.L.; formal analysis, Y.W.; investigation, L.W., Z.H. and Y.L.; resources, J.G., A.L. and X.G.; data curation, Y.W. and X.G.; writing—original draft preparation, Y.W.; writing—review and editing, Y.W., A.L. and X.G.; visualization, L.Y.; supervision, J.G. and X.G.; project administration, Y.W. and X.G.; funding acquisition, Y.W. and X.G. All authors have read and agreed to the published version of the manuscript.

Funding: This research was funded by the Xinjiang Uygur Autonomous Region Natural Science Foundation (2020D01B64), the Chinese National Natural Science Foundation (22008257), the Technology Innovation Program of Karamay (2020CGZH0001), the Youth Foundation of the University Research Program of Xinjiang Uygur Autonomous Region (XJEDU2020Y044) and the Research Foundation of China University of Petroleum-Beijing at Karamay (XQZX20190043).

Institutional Review Board Statement: Not applicable.

Informed Consent Statement: Not applicable.

Data Availability Statement: Not applicable.

Acknowledgments: This work was supported by the Xinjiang Uygur Autonomous Region Natural Science Foundation (2020D01B64), the Chinese National Natural Science Foundation (22008257), the Technology Innovation Program of Karamay (2020CGZH0001), the Youth Foundation of the University Research Program of Xinjiang Uygur Autonomous Region (XJEDU2020Y044) and the Research Foundation of China University of Petroleum-Beijing at Karamay (XQZX20190043), which are greatly acknowledged.

Conflicts of Interest: The authors declare no conflict of interest.

References

1. Sloan, E.D. Fundamental principles and applications of natural gas hydrates. *Nature* **2003**, *426*, 353–363. [CrossRef] [PubMed]
2. Zheng, J.J.; Loganathan, N.K.; Zhao, J.Z.; Linga, P. Clathrate hydrate formation of CO_2/CH_4 mixture at room temperature: Application to direct transport of CO_2-containing natural gas. *Appl. Energy* **2019**, *249*, 190–203. [CrossRef]
3. Rajput, F.; Maric, M.; Servio, P. Amphiphilic Block Copolymers with Vinyl Caprolactam as Kinetic Gas Hydrate Inhibitors. *Energies* **2021**, *14*, 341. [CrossRef]
4. Zaripova, Y.; Yarkovoi, V.; Varfolomeev, M.; Kadyrov, R.; Stoporev, A. Influence of Water Saturation, Grain Size of Quartz Sand and Hydrate-Former on the Gas Hydrate Formation. *Energies* **2021**, *14*, 1272. [CrossRef]
5. Xu, C.G.; Wang, M.; Xu, G.; Li, X.S. The Relationship between Thermal Characteristics and Microstructure/Composition of Carbon Dioxide Hydrate in the Presence of Cyclopentane. *Energies* **2021**, *14*, 870. [CrossRef]
6. Liu, H.; Guo, P.; Zhan, S.; Ma, P.; Wei, N.; Zhao, J.; Qiu, Y. Experimental investigation into formation/dissociation characteristics of methane hydrate in consolidated sediments with resistance measurement. *Fuel* **2018**, *234*, 985–995. [CrossRef]
7. Molokitina, N.S.; Nesterov, A.N.; Podenko, L.S.; Reshetnikov, A.M. Carbon dioxide hydrate formation with SDS: Further insights into mechanism of gas hydrate growth in the presence of surfactant. *Fuel* **2019**, *235*, 1400–1411. [CrossRef]
8. Chao, C.; Fan, W.; Tian, Y.; Wu, X.; Zhang, J.; Zhang, J.; Li, L.; Yang, P.; Zhao, J. Review and prospects of hydrate cold storage technology. *Renew. Sustain. Energy Rev.* **2020**, *117*, 109492.
9. Liu, H.; Zhan, S.; Li, R.; Liu, Y.; Guo, P.; Wang, Z.; Du, J.; Wen, Y.; Dai, P.; Liao, H. High-efficiency natural-gas storage method involving formation of gas hydrate in water/oil-cyclopentane emulsion. *Chem. Eng. J.* **2020**, *400*, 125369. [CrossRef]
10. Zhang, L.; Kuang, Y.; Dai, S.; Wang, J.; Zha, J.; Song, Y. Kinetic enhancement of capturing and storing greenhouse gas and volatile organic compound: Micro-mechanism and micro-structure of hydrate growth. *Chem. Eng. J.* **2020**, *379*, 122357. [CrossRef]
11. Zhang, Q.; Zheng, J.; Zhang, B.; Linga, P. Coal mine gas separation of methane via clathrate hydrate process aided by tetrahydrofuran and amino acids. *Appl. Energy* **2021**, *287*, 116576. [CrossRef]
12. Linga, P.; Clarke, M.A. A Review of Reactor Designs and Materials Employed for Increasing the Rate of Gas Hydrate Formation. *Energy Fuels* **2017**, *31*, 1–13. [CrossRef]
13. Liu, L.; Yao, Y.; Zhou, X.; Zhang, Y.; Liang, D. Improved Formation Kinetics of Carbon Dioxide Hydrate in Brine Induced by Sodium Dodecyl Sulfate. *Energies* **2021**, *14*, 2094. [CrossRef]
14. Liu, F.P.; Li, A.R.; Wang, J.; Luo, Z.D. Iron-based ionic liquid ([BMIM][$FeCl_4$]) as a promoter of CO_2 hydrate nucleation and growth. *Energy* **2021**, *214*, 119034. [CrossRef]
15. Wang, Y.W.; Yang, B.; Liu, Z.Q.; Liu, Z.Q.; Sun, Q.; Liu, A.X.; Li, X.X.; Lan, W.J.; Yang, L.Y.; Guo, X.Q. The hydrate-based gas separation of hydrogen and ethylene from fluid catalytic cracking dry gas in presence of Poly (sodium 4-styrenesulfonate). *Fuel* **2020**, *275*, 117895. [CrossRef]
16. Wang, X.L.; Zhang, F.Y.; Lipiński, W. Research progress and challenges in hydrate-based carbon dioxide capture applications. *Appl. Energy* **2020**, *269*, 114928. [CrossRef]

17. Dicharry, C.; Diaz, J.; Torré, J.P.; Ricaurte, M. Influence of the carbon chain length of a sulfate-based surfactant on the formation of CO_2, CH_4 and CO_2–CH_4 gas hydrates. *Chem. Eng. Sci.* **2016**, *152*, 736–745. [CrossRef]
18. Li, S.R.; Liu, S.C.; Fu, Z.W.; Li, Q.Y.; Wu, C.F.; Guo, W.H. Surface modification and characterization of carbon black by sodium lignosulphonate. *Surf. Interface Anal.* **2017**, *49*, 197–204. [CrossRef]
19. Duan, J.T.; Litwiller, E.; Choi, S.H.; Pinnau, I. Evaluation of sodium lignin sulfonate as draw solute in forward osmosis for desert restoration. *J. Membrane Sci.* **2014**, *453*, 463–470. [CrossRef]
20. Zang, X.Y.; Wan, L.H.; He, Y.; Liang, D.Q. CO_2 removal from synthesized ternary gas mixtures used hydrate formation with sodium dodecyl sulfate (SDS) as additive. *Energy* **2020**, *190*, 116399–116409. [CrossRef]
21. Mofrad, H.R.; Ganji, H.; Nazari, K.; Kameli, M.; Rod, A.R.; Kakavand, M. Rapid formation of dry natural gas hydrate with high capacity and low decomposition rate using a new effective promoter. *J. Petrol. Sci. Eng.* **2016**, *147*, 756–759. [CrossRef]
22. Song, Y.M.; Liang, R.Q.; Wang, F.; Zhang, D.H.; Yang, L.; Zhang, D.B. Enhanced methane hydrate formation in the highly dispersed carbon nanotubes-based nanofluid. *Fuel* **2021**, *285*, 119234. [CrossRef]
23. Lv, D.; Li, Y.; Wang, L.J. Carbon aerogels derived from sodium lignin sulfonate embedded in carrageenan skeleton for methylene-blue removal. *Int. J. Biol. Macromol.* **2020**, *148*, 979–987. [CrossRef] [PubMed]
24. Yang, H.T.; Yu, B.; Xu, X.D.; Bourbigot, S.; Wang, H.; Song, P.G. Lignin-derived bio-based flame retardants toward high-performance sustainable polymeric materials. *Green Chem.* **2020**, *22*, 2129–2161. [CrossRef]
25. Yi, J.; Zhong, D.L.; Yan, J.; Lu, Y.Y. Impacts of the surfactant sulfonated lignin on hydrate based CO_2 capture from a CO_2/CH_4 gas mixture. *Energy* **2019**, *171*, 61–68. [CrossRef]
26. Shi, L.L.; Ding, J.X.; Liang, D.Q. Enhanced CH_4 storage in hydrates with the presence of sucrose stearate. *Energy* **2019**, *180*, 978–988. [CrossRef]
27. Chen, G.J.; Sun, C.Y.; Ma, Q.L. *Science and Technology of Gas Hydrate*, 1st ed.; Chemical Industry Press: Beijing, China, 2008.
28. Yu, C.H.; Chen, L.T.; Sun, B.J. Experimental characterization of guest molecular occupancy in clathrate hydrate cages: A review. *Chin. J. Chem. Eng.* **2019**, *27*, 2189–2206. [CrossRef]
29. Hassanpouryouzband, A.; Joonaki, E.; Farahani, M.V.; Takeya, S.; Ruppel, C.; Yang, J.; English, N.J.; Schicks, J.M.; Edlmann, K.; Mehrabian, H.; et al. Gas hydrates in sustainable chemistry. *Chem. Soc. Rev.* **2020**, *49*, 5225–5309. [CrossRef]
30. Asadi, F.; Ejtemaei, M.; Birkett, G.; Searles, D.J.; Nguyen, A.V. The link between the kinetics of gas hydrate formation and surface ion distribution in the low salt concentration regime. *Fuel* **2019**, *240*, 309–316. [CrossRef]
31. Van der Waals, J.H.; Platteeuw, J.C. Clathrate Solutions. *Adv. Chem. Phys.* **1959**, *2*, 1–57.
32. Chen, G.J.; Guo, T.M. Thermodynamic modeling of hydrate formation based on new concepts. *Fluid Phase Equilibr.* **1996**, *122*, 43–65. [CrossRef]
33. Belosludov, R.V.; Zhdanov, R.K.; Gets, K.V.; Bozhko, Y.Y.; Belosludov, V.R.; Kawazoe, Y. Role of Methane as Second Guest Component in Thermodynamic Stability and Isomer Selectivity of Butane Clathrate Hydrates. *J. Phys. Chem. C* **2020**, *124*, 18474–18481. [CrossRef]
34. Belosudov, R.V.; Subbotin, O.S.; Mizuseki, H.; Kawazoe, Y.; Belosludov, V.R. Accurate description of phase diagram of clathrate hydrates at the molecular level. *J. Phys. Chem. C* **2009**, *131*, 244510. [CrossRef]
35. Kodera, M.; Matsueda, T.; Belosludov, R.V.; Zhdanov, R.K.; Belosludov, V.R.; Takeya, S.; Alavi, S.; Ohmura, R. Physical Properties and Characterization of the Binary Clathrate Hydrate with Methane + 1,1,1,3,3-Pentafluoropropane (HFC-245fa) + Water. *J. Phys. Chem. C* **2020**, *124*, 20736–20745. [CrossRef]
36. Belosludov, V.R.; Subbotin, O.S.; Krupskii, D.S.; Belosludov, R.V.; Kawazoe, Y.; Kudoh, J. Physical and Chemical Properties of Gas Hydrates: Theoretical Aspects of Energy Storage Application. *Mater. Trans.* **2007**, *48*, 704–710. [CrossRef]
37. Bozhko, Y.Y.; Subbotin, O.S.; Belosludov, V.R.; Mizuseki, H.; Kawazoe, Y.; Fomin, V.M. Stability and Composition of Helium Hydrates Based on Ices Ih and II at Low Temperatures. *J. Phys. Chem. C* **2014**, *118*, 2587–2593.
38. Subbotin, O.S.; Adamova, T.P.; Belosludov, V.R.; Mizuseki, H.; Kawazoe, Y.; Kudoh, J.; Rodger, P.M.; Belosludov, V.R. Theoretical study of phase transitions in Kr and Ar clathrate hydrates from structure II to structure I under pressure. *J. Phys. Chem. C* **2009**, *131*, 114507. [CrossRef] [PubMed]
39. Chen, G.J.; Guo, T.M. A new approach to gas hydrate modelling. *Chem. Eng. J.* **1998**, *71*, 145–151. [CrossRef]
40. Xu, Z.; Sun, Q.; Gao, J.; Liu, Z.; Zhang, J.; Wang, Y.; Guo, X.; Liu, A.; Yang, L. Experiment and model investigation of D-sorbitol as a thermodynamic hydrate inhibitor for methane and carbon dioxide hydrates. *J. Nat. Gas Sci. Eng.* **2021**, *90*, 103927. [CrossRef]
41. Xu, Z.; Sun, Q.; Wang, Y.; Luo, Y.; Yue, G.; Guo, X.; Li, X.; Yang, L. Experimental and modelling study on the effect of maltose as a green additive on methane hydrate. *J. Chem. Thermodyn.* **2020**, *144*, 105980. [CrossRef]
42. Li, N.; Zhang, C.W.; Ma, Q.L.; Sun, Z.F.; Chen, Y.; Jia, S.; Chen, G.J.; Sun, C.Y.; Yang, L.Y. Measurements and modeling of interfacial tension for (CO_2 + n-alkyl benzene) binary mixtures. *J. Supercrit. Fluid* **2019**, *154*, 104625–104633. [CrossRef]
43. Qin, H.B.; Sun, C.Y.; Sun, Z.F.; Liu, B.; Chen, G.J. Relationship between the interfacial tension and inhibition performance of hydrate inhibitors. *Chem. Eng. Sci.* **2016**, *148*, 182–189. [CrossRef]
44. Patel, N.C.; Teja, A.S. A new cubic equation of state for fluids and fluid mixtures. *Chem. Eng. Sci.* **1982**, *37*, 463–473. [CrossRef]
45. Zuo, Y.X.; Guo, T.M. Extension of the Patel—Teja equation of state to the prediction of the solubility of natural gas in formation water. *Chem. Eng. Sci.* **1991**, *46*, 3251–3258. [CrossRef]
46. Jarrahiana, A.; Nakhaee, A. Hydrate–liquid–vapor equilibrium condition of N_2 + CO_2 + H_2O system: Measurement and modeling. *Fuel* **2019**, *237*, 769–774. [CrossRef]

47. Liu, H.; Guo, P.; Du, J.; Wang, Z.; Chen, G.; Li, Y. Experiments and modeling of hydrate phase equilibrium of $CH_4/CO_2/H_2S/N_2$ quaternary sour gases in distilled water and methanol-water solutions. *Fluid Phase Equilibr.* **2017**, *432*, 10–17. [CrossRef]
48. Sun, J.Y.; Xin, Y.; Chou, I.M.; Sun, R.; Jiang, L. Hydrate Stability in the H_2S-H_2O system-Visual Observations and Measurements in a High-Pressure Optical Cell and Thermodynamic Models. *J. Chem. Eng. Data* **2020**, *65*, 3884–3892. [CrossRef]
49. Abudu, R.T.; Sun, Q.; Xu, Z.; Guo, X.Q.; Yang, L.Y. Two-Stage Separation of the Tail Gases of Ammonia Synthesis to Recover H_2 and N_2 via Hydrate Formation. *J. Chem. Eng. Data* **2020**, *65*, 1715–1720. [CrossRef]
50. Ma, Q.L.; Qi, J.L.; Chen, G.J.; Sun, C.Y. Modeling study on phase equilibria of semiclathrate hydrates of pure gases and gas mixtures in aqueous solutions of TBAB and TBAF. *Fluid Phase Equilibr.* **2016**, *430*, 178–187. [CrossRef]
51. Hu, Y.; Lee, B.R.; Sum, A.K. Universal correlation for gas hydrates suppression temperature of inhibited systems: I. Single salts. *AIChE J.* **2017**, *63*, 5111–5124. [CrossRef]
52. Wang, Y.W.; Deng, Y.; Guo, X.Q.; Sun, Q.; Liu, A.X.; Zhang, G.Q.; Yue, G.; Yang, L.Y. Experimental and modeling investigation on separation of methane from coal seam gas (CSG) using hydrate formation. *Energy* **2018**, *150*, 377–395. [CrossRef]
53. Luo, H.; Sun, C.Y.; Huang, Q.; Peng, B.Z.; Chen, G.J. Interfacial tension of ethylene and aqueous solution of sodium dodecyl sulfate (SDS) in or near hydrate formation region. *J. Colloid Interface Sci.* **2006**, *297*, 266–270. [CrossRef]
54. Mańko, D.; Zdziennicka, A.; Jańczuk, B. Surface and volumetric properties of n-octyl-β-D-glucopyranoside and rhamnolipid mixture. *J. Mol. Liq.* **2016**, *219*, 801–809. [CrossRef]
55. Gayet, P.; Dicharry, C.; Marion, G.; Graciaa, A.; Lachaise, J.; Nesterov, A. Experimental determination of methane hydrate dissociation curve up to 55 MPa by using a small amount of surfactant as hydrate promoter. *Chem. Eng. Sci.* **2005**, *60*, 5751–5758. [CrossRef]
56. Liu, H.; Zhan, S.; Guo, P.; Fan, S.; Zhang, S. Understanding the characteristic of methane hydrate equilibrium in materials and its potential application. *Chem. Eng. J.* **2018**, *349*, 775–781. [CrossRef]
57. Cheng, L.W.; Liao, K.; Li, Z.; Cui, J.L.; Liu, B.; Li, F.G.; Chen, G.J.; Sun, C.Y. The invalidation mechanism of kinetic hydrate inhibitors under high subcooling conditions. *Chem. Eng. Sci.* **2019**, *207*, 305–316. [CrossRef]
58. Li, Z.; Liao, K.; Qin, H.B.; Chen, J.L.; Ren, L.L.; Li, F.G.; Zhang, X.R.; Liu, B.; Chen, G.J. The gas-adsorption mechanism of kinetic hydrate inhibitors. *AIChE J.* **2019**, *65*, 16681. [CrossRef]
59. Ando, N.; Kuwabara, Y.; Mori, Y.H. Surfactant effects on hydrate formation in an unstirred gas/liquid system: An experimental study using methane and micelle-forming surfactants. *Chem. Eng. Sci.* **2012**, *73*, 79–85. [CrossRef]
60. Zhong, D.L.; Li, Z.; Lu, Y.Y.; Wang, J.L.; Yan, J. Evaluation of CO_2 removal from a CO_2+ CH_4 gas mixture using gas hydrate formation in liquid water and THF solutions. *Appl. Energy* **2015**, *158*, 133–141. [CrossRef]